Magnetic Resonance Imaging Characteristics Predict Epidermal Growth Factor Receptor Amplification Status in Glioblastoma

Manish Aghi,[1] Paola Gaviani,[2,5] John W. Henson,[2,3] Tracy T. Batchelor,[2,6] David N. Louis,[1,4,6] and Fred G. Barker II[1]

Abstract

Purpose: Two clinical-molecular glioblastoma subtypes have been described: "primary" glioblastomas arise *de novo* in older patients and often overexpress epidermal growth factor receptor (*EGFR*); "secondary" glioblastomas progress from lower-grade tumors in younger patients and commonly have *TP53* mutations. *EGFR* overexpression correlates in experimental gliomas with increased angiogenesis, edema, and invasion. No radiographic predictors of molecular glioblastoma subtype are known.

Experimental Design: We retrospectively reviewed 75 glioblastomas, classified as *TP53*-mutated (n = 11), *EGFR*-amplified (n = 31), or neither (non-*TP53*/non-*EGFR*; n = 33). Four variables were derived from preoperative magnetic resonance imaging: (*a*) T2/T1, the ratio of T2-bright volume to enclosed T1-enhancing volume; (*b*) percentage of tumor volume that was necrosis; and (*c* and *d*) T1 and T2 border sharpness coefficients (BSC), the rates of change in grayscale intensity of adjacent 0.02-cm^2 voxels traversing the anterior, posterior, and lateral borders on T1-enhanced and T2 images.

Results and Conclusions: Mean T2/T1 was 4.7 for *EGFR*-amplified glioblastomas, greater than that of *TP53*-mutated glioblastomas (2.3) or non-*TP53*/non-*EGFR* glioblastomas (2.6; $P < 0.00005$). All four tumors with T2/T1 > 7.2 were *EGFR*-amplified; 0 of 15 with T2/T1 < 4.7 underwent gross total resection. The mean T2 BSC of *EGFR*-amplified glioblastomas was 33.7, less sharp ($P < 0.0000005$) than *TP53*-mutated (72.2) and non-*TP53*/non-*EGFR* glioblastomas (81.2). All 15 glioblastomas with T2 BSC < 30.8 were *EGFR*-amplified. Percentage necrosis and T1 BSC did not differ between glioblastoma subtypes. The increased T2/T1 ratio and decreased T2 BSC in *EGFR*-overexpressing tumors are the first radiographic distinctions described between glioblastoma molecular subtypes. These findings may reflect increased angiogenesis, edema, and/or invasion in *EGFR*-overexpressing tumors.

Despite aggressive management with surgery, radiation, and chemotherapy, the prognosis for patients with glioblastoma remains poor. Median survival is typically <1 year with little change in several decades (1).

Two clinical-molecular glioblastoma subtypes have been described: "primary" glioblastomas arise *de novo* in older patients and often overexpress epidermal growth factor receptor (*EGFR*); "secondary" glioblastomas progress from lower-grade tumors in younger patients and commonly have *TP53* mutations (2). Numerous phenotypic differences between these two genetic subtypes of glioblastoma have been described. The differences in patient age have already been noted (2). *EGFR*-amplified glioblastomas are relatively radiation resistant (3) and recur more rapidly after treatment (4). Histopathologically, in model systems, *EGFR*-amplified glioblastomas display increased angiogenesis, edema, and brain invasion (5).

To date, the molecular subtypes of glioblastoma can only be identified by genetic analysis of surgical specimens. A radiographic predictor of glioblastoma subtype would potentially be of value for several reasons. First, there remains disagreement about the optimal molecular method by which to determine EGFR status (6). Second, preclinical studies of EGFR-targeted therapies suggest that sensitivity to these agents may correlate with alterations in downstream signaling pathways better than with *EGFR* expression itself (7, 8). A radiographic variable might better reflect these downstream pathways than *EGFR* amplification or expression levels. Third, with increased development of targeted therapies, the genetic subtype of glioblastoma may eventually affect treatment choices, including the delivery of surgically implanted agents for which a preoperative decision about use could be facilitated by a radiographic predictor of molecular status.

Authors' Affiliations: [1]Neurosurgical Service; Departments of [2]Neurology, [3]Neuroradiology, and [4]Pathology; [5]Stephen E. and Catherine Pappas Center for Neuro-Oncology; and [6]Molecular Neuro-Oncology Laboratory, Massachusetts General Hospital and Harvard Medical School Boston, Massachusetts

Received 3/31/05; revised 8/9/05; accepted 9/1/05.

Grant support: NIH grant CA57683 (D.N. Louis).

The costs of publication of this article were defrayed in part by the payment of page charges. This article must therefore be hereby marked *advertisement* in accordance with 18 U.S.C. Section 1734 solely to indicate this fact.

Requests for reprints: Manish Aghi, Department of Neurosurgery, Massachusetts General Hospital, Room 502, White Building, 55 Fruit Street, Boston, MA 02114. Phone: 617-840-5111; Fax: 617-726-5677; E-mail: maghi@partners.org.

doi:10.1158/1078-0432.CCR-05-0713

Because *EGFR* amplification seems to be selected for in the infiltrating edges of glioblastoma (9) and because EGFR gene amplification seems to up-regulate invasion-associated genes (5), we hypothesized that aspects of standard magnetic resonance imaging (MRI) that can reflect edema and infiltrating tumor cells in the volume surrounding solid glioblastoma tumors might predict *EGFR* amplification status (10). Specifically, we studied aspects of the T2-bright tissue volume that surrounds the T1-enhancing solid tumor. The T2-bright volume represents a combination of edema and infiltrating tumor cells adjacent to solid T1-enhancing glioblastoma tissue (10). We compared the volume of T2-bright tissue to the T1-enhancing solid tumor volume and also studied the sharpness of the borders between T1-enhancing and T2-bright volumes and adjacent tissue.

Materials and Methods

Patients. The study was based on a previously described consecutive series of 140 patients with glioblastoma treated by a surgical procedure at our institution (11). From the original series of 140 patients, 75 with preoperative MRIs completed at our institution, showing a gadolinium-enhancing lesion before the administration of steroids, were included in the study. Postoperative MRIs were used to determine extent of surgical resection. Records were reviewed to confirm each patient's surgical procedure. This study was approved by the Institutional Review Board of Massachusetts General Hospital.

Molecular data. Tumor DNA was extracted from microdissected, formalin-fixed, paraffin-embedded sections. Glioblastomas were classified as *TP53*-mutated, *EGFR*-amplified, or neither (non-*TP53*/non-*EGFR*) on the basis of single-strand conformational polymorphism and direct sequencing of exons 5 through 8 of the *TP53* gene and differential PCR for *EGFR* in tumor versus blood lymphocytes (12). The EGFR variant III mutation was not specifically evaluated.

Radiographic analysis. Three-dimensional volumetric analysis was done on preoperative MRIs using Vitrea 2 computer software (Vital Images, Inc., Plymouth, MN; 2003). The observer was blinded to molecular analysis results. The ratio of T2-bright volume to the enclosed T1-enhancing volume (including internal necrosis), T2/T1, was calculated (Fig. 1). T2/T1 derivation took ~5 minutes per tumor.

The percent necrosis was calculated as 100 × [(T1 hypodense nonenhancing areas surrounded by ring enhancement) / (T1-enhancing areas + T1 nonenhancing areas surrounded by ring enhancement)]. T2 sequences were used to confirm that "necrotic areas" did not represent cysts.

The T1 and T2 border sharpness coefficients (BSC) were calculated by applying the following algorithm to the T1 gadolinium-enhanced and T2 axial images with the largest T1-enhancing or T2-bright areas: (*a*) three (T1 gadolinium-enhanced) or four (T2) adjacent 0.02-cm^2 circular voxels were placed progressively from outside the area of gadolinium-enhancement or T2 brightness working inward, starting with a voxel that was as close to the bright area as possible with average grayscale units statistically comparable ($P > 0.05$ by two-sample t test using the number of pixels in each voxel, the average grayscale intensity of the 4 to 12 pixels in each voxel, and the SD of the grayscale units of the pixels in each voxel) to the same space in the contralateral hemisphere; the average grayscale units contained within each of the voxels was then recorded; (*b*) the slope of a linear regression correlating average grayscale unit with voxel number (one to four) was calculated; (*c*) the average of the four slopes at the anterior, posterior, right, and left tumor borders, excluding borders that abutted ventricles or cortical surfaces, was the BSC, with higher BSC signifying a sharp border and lower BSC a fuzzy border (Fig. 2). Calculation of each BSC took ~5 minutes per tumor. To confirm interobserver reproducibility of T1 and T2 BSCs, a second observer, also blinded to the results of molecular analysis, derived T1 and T2 BSCs for each tumor. The second observer verified that T1 BSC did not differ between glioblastoma subtypes whereas T2 BSC was less in *EGFR*-amplified than in non-*EGFR*-amplified glioblastomas ($P < 0.02$). κ statistics, derived by stratifying the BSCs of each observer into quintiles, were 0.4 for T1 BSC and 0.5 for T2 BSC, confirming significant interobserver reproducibility ($P < 0.00001$).

Statistical analysis. S-plus software was used to derive κ statistics to assess interobserver variability and receiver operating characteristic curves for T2/T1 and T2 BSC analysis. The log-rank test was used to

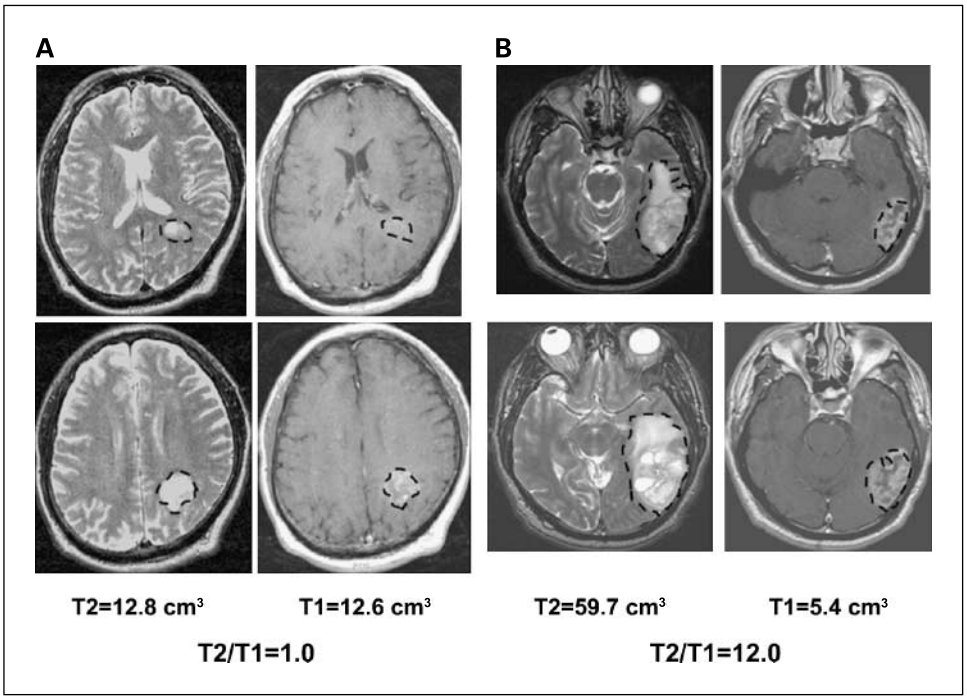

Fig. 1. Method of calculating T2/T1 ratio. Vitrea 2 computer software was used to derive three-dimensional volumes of T2 brightness and enclosed T1-enhancing volume (including internal necrosis). The ratio of these volumes was the T2/T1 ratio. The software outlines the areas of abnormality on each axial image and the user can modify any incorrectly labeled areas. The volume is then derived by the program using the total areas of abnormalities and the thickness of each axial image. Two representative T2 (left two images in *A* and *B*) and T1-enhanced (right two images in *A* and *B*) axial images from two tumors (*A* and *B*), one of which (*A*) had a low T2/T1 ratio and proved to be non-*EGFR*-amplified whereas the other (*B*) had a high T2/T1 ratio and proved to be *EGFR*-amplified.

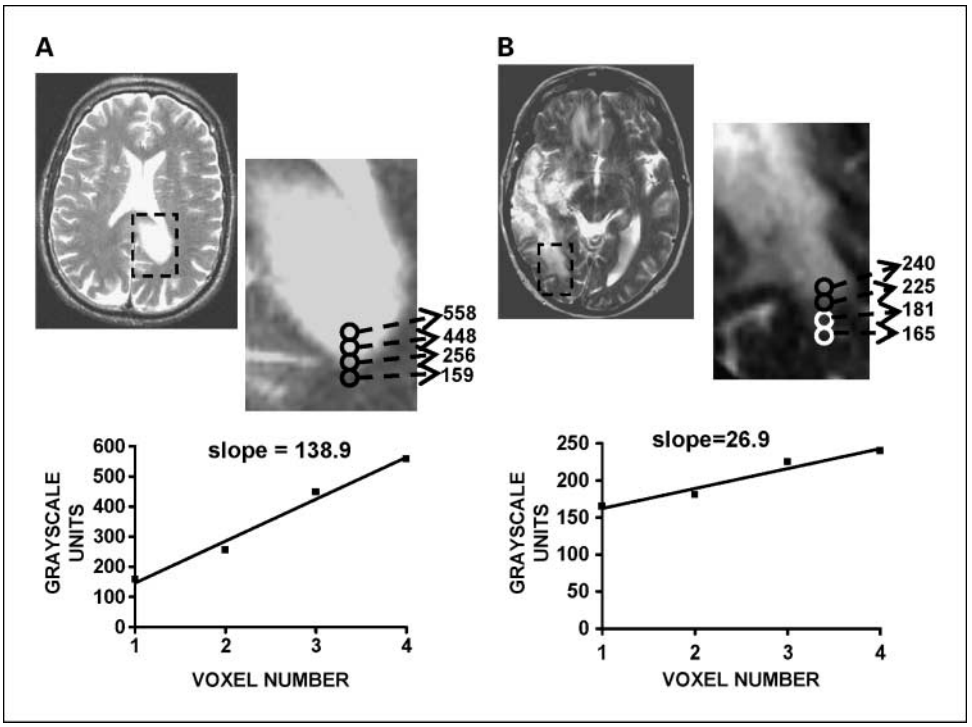

Fig. 2. Method of calculating BSC. To calculate T2 BSC, four adjacent 0.02-cm^2 voxels were placed along a line perpendicular to the anterior, posterior, and lateral tumor borders on the axial image containing the largest T2-bright area. Axial T2 images with the largest area of abnormality from two different tumors (*A* and *B*). The posterior T2 bright borders are enlarged. The first voxel is placed as close to the edge of T2 brightness as possible such that its grayscale units do not deviate from that of a voxel in the same position in the contralateral hemisphere. This first voxel is followed by three more adjacent voxels running posterior to anterior. The slope of a linear regression connecting the grayscale units of the four voxels is derived. The process is repeated for the three other borders (except for borders that lie on cortical surfaces or against ventricles) and the T2 BSC is the average of the slopes at each border. The tumor shown in (*A*) had the largest T2 BSC, signifying a sharp T2 bright border, and proved to be non-*EGFR*-amplified, whereas the tumor in (*B*) had the smallest T2 BSC, signifying a fuzzy T2 bright border, and proved to be *EGFR*-amplified. For T1 BSC, three adjacent voxels were used on the axial image containing the largest gadolinium-enhanced area.

compare Kaplan-Meier survival curves of glioblastoma subgroups. Spearman's rank correlation coefficient was used to quantify the correlation between ordinal data such as age, T2/T1, T1-enhancing volume, T2 BSC, and percent necrosis. Student's *t* test was used as a parametric test to compare the differences in the radiographic variables (T1 BSC, percent necrosis) between glioblastoma subtypes. ANOVA was used to compare the features of tumors in each of the four lobes. For nonparametric comparisons (T2/T1, T2 BSC), the Kruskal-Wallis test was used to compare multiple groups and the Mann-Whitney *U* test was used to compare two groups.

Results

Basic MRI findings of the molecular glioblastoma subtypes. There were 31 *EGFR*-amplified, 11 *TP53*-mutated, and 33 non-*TP53*/non-*EGFR* glioblastomas with mean T1-enhancing volumes (including internal necrosis) of 31.2, 30.9, and 44.0 cm^3, respectively ($P > 0.05$). These tumors were then analyzed for four radiographic variables that could be derived from their T1 and T2 studies—T2/T1 ratio, percent necrosis, and T1 and T2 BSCs.

T2/T1 ratio of molecular glioblastoma subtypes. T2-bright tissue volumes at the margins of malignant gliomas reflect edema and tumor invasion (10). We compared the T2/T1 ratio, the ratio of T2-bright volume to enclosed T1-enhancing volume (Fig. 1), between molecular glioblastoma multiforme subtypes. T2/T1 ratio was significantly greater in *EGFR*-amplified glioblastomas than in the other groups ($P < 0.00005$, Mann-Whitney *U* test). Mean T2/T1 was 4.7 for *EGFR*-amplified glioblastomas (range 1.3-15), 2.3 for *TP53*-mutated glioblastomas (1.0-4.8), and 2.6 for non-*TP53*/non-*EGFR* glioblastomas (1.0-7.2; Fig. 3A). All four tumors with T2/T1 > 7.2 (5% of the tumors analyzed) were *EGFR*-amplified.

T2/T1 decreased as T1 volume increased and increased with the patient's age, but neither tendency was statistically significant ($P > 0.05$, Spearman's rank correlation). Nine of 44 non-*EGFR*-amplified glioblastomas (20.5%) underwent gross total resection, exceeding the 4 of 31 *EGFR*-amplified glioblastomas (12.9%) that received gross total resection ($P = 0.37$). None of 15 tumors (20% of the tumors analyzed) with T2/T1 > 4.7 underwent gross total resection. T2/T1 did not correlate with survival ($P > 0.05$)—the median survival of patients with T2/T1 > 3 (the median for all glioblastomas in this report) was 362 days, compared with 385 days for patients with T2/T1 < 3 ($P > 0.05$). Average T2/T1 values were 4.9, 3.7, 3.0, and 2.7 for lesions involving the parietal, temporal, occipital, and frontal lobes, respectively ($P = 0.056$ for global comparison of the four groups by ANOVA; $P = 0.007$ for parietal versus frontal, $P = 0.03$ for parietal versus occipital, and $P > 0.05$ for all other comparisons).

Percent necrosis found in molecular glioblastoma subtypes. The exact mechanisms of glioblastoma necrosis have not been identified. To determine whether *EGFR* amplification or *TP53* mutations are associated with glioblastoma necrosis, we compared the percentage of radiographic necrosis found in the molecular glioblastoma subtypes by calculating the percentage of total T1 tumor volume that had a hypodense appearance contained within an enhancing border. The percent necrosis did not vary with glioblastoma subtype, averaging 29.7%, 24.0%, and 26.2% for *EGFR*-amplified (range, 0-80%), *TP53*-mutated (range, 0-74.4%), and non-*TP53*/non-*EGFR* (range, 0-71.3%) glioblastomas, respectively. Necrosis also did not correlate with survival—the median survival of patients whose tumors exhibited >22.5% necrosis (the median necrosis) was 365 days, virtually identical to the 364-day median survival of patients with tumors exhibiting <22.5% necrosis. The median survival of the seven patients with no radiographic necrosis was 363 days, virtually identical to the 365-day median survival of the 68 patients who did have radiographic necrosis.

T1 BSC of the molecular glioblastoma subtypes. Next, we derived the T1 BSC, the slope of a linear regression connecting

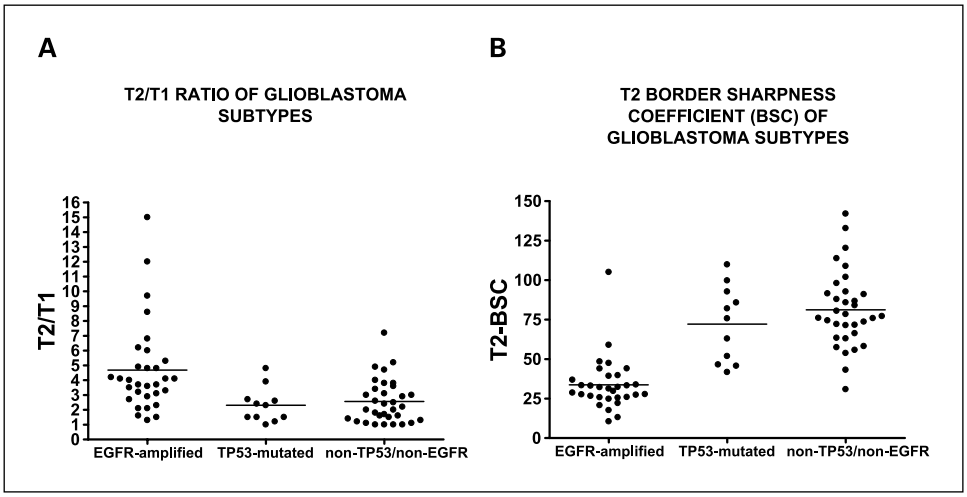

Fig. 3. Scatter plot showing T2/T1 ratio (*A*) and T2 BSC (*B*) of the glioblastomas in this report. Horizontal bars, means of the three glioblastoma subtypes: *EGFR*-amplified, *TP53*-mutated, and non-*EGFR*/non-*TP53*. T2/T1 ratio was significantly higher ($P < 0.00005$, Mann-Whitney *U* test) and T2 BSC was significantly lower ($P < 0.0000005$, Mann-Whitney *U* test) in *EGFR*-amplified than in non-*EGFR* amplified glioblastomas.

the grayscale units of three sequential 0.02-cm^2 voxels traversing from just outside to inside the T1-enhancing edges at the anterior, posterior, and two lateral borders of T1 enhancement. T1 BSC did not vary significantly with glioblastoma subtype, averaging 113.0, 83.8, and 111.2 for *EGFR*-amplified, *TP53*-mutated, and non-*TP53*/non-*EGFR* glioblastomas, respectively ($P > 0.05$). T1 BSC also did not affect survival—the median survival of patients whose tumors had T1 BSCs < 99.1 (the median T1 BSC) was 365 days, comparable to the 364-day median survival of patients whose tumors had T1 BSCs ≥ 99.1.

T2 BSC of the molecular glioblastoma subtypes. Similarly, the T2 BSC was derived using the axial T2 image containing the largest T2-bright area (Fig. 2). The mean T2 BSC of *EGFR*-amplified glioblastomas was 33.7, significantly less than the values for *TP53*-mutated (72.2) and non-*TP53*/non-*EGFR* glioblastomas (81.2; $P < 0.0000005$, Mann-Whitney *U* test; Fig. 3B). All 15 glioblastomas with T2 BSC < 30.8 (20% of tumors analyzed) were *EGFR*-amplified. T2 BSC did not correlate with survival—patients whose glioblastomas had T2 BSCs < 57.4 (the median T2 BSC) had a median survival of 345 days, comparable to the 385-day median survival of patients whose glioblastomas had T2 BSCs > 57.4 ($P > 0.05$). T2 BSC also did not correlate with anatomic location of glioblastoma—the mean T2 BSCs for tumors involving the parietal, temporal, occipital, and frontal lobes were 48.4, 58.7, 60.0, and 61.3, respectively ($P = 0.5$, ANOVA). T2 BSC decreased with increasing T2/T1 ratio in a significant manner ($P = 0.048$). Although T2 BSC tended to decrease with increasing patient age, the tendency was not significant ($P = 0.2$).

Receiver operating characteristic curves for T2/T1 and T2 BSC. Receiver operating characteristic curves, which depict the tradeoff between sensitivity and specificity, were generated for T2/T1 and T2 BSC in this cohort (Fig. 4). Areas under receiver operating characteristic curves can range from 0.5, when a test has 50% sensitivity and 50% specificity and is no better than random chance, to 1.0 for a test with perfect discrimination because it achieves both 100% sensitivity and 100% specificity. The area under the T2/T1 receiver operating characteristic curve was 0.78 whereas the area under the T2 BSC receiver operating characteristic curve was 0.92 (Fig. 4), confirming the degree to which both variables balanced sensitivity and specificity, T2 BSC > T2/T1.

Discussion

Several phenotypic differences between primary and secondary glioblastoma subtypes have been previously described. First, there are differences in the patient populations, with *EGFR*-amplified glioblastomas affecting an older population and more often representing *de novo* tumors (2). Second, there are biological differences, with *EGFR*-amplified glioblastomas exhibiting increased angiogenesis, likely due to increased secretion of vascular endothelial growth factor (13), and increased brain invasion, likely due to increased secretion of matrix metalloproteinases (14). Third, there are differences in outcome, with *EGFR*-amplified glioblastomas being potentially more resistant to radiation (3), undergoing more rapid postoperative regrowth (4), and displaying improved survival in older patients but worse survival in younger patients if *TP53* is not mutated (15).

Here, we report the first findings of radiographic differences between molecular glioblastoma subtypes: increased T2/T1 ratio and decreased T2 BSC (fuzzier borders) in tumors overexpressing *EGFR*. T2-bright tissue volume surrounding a

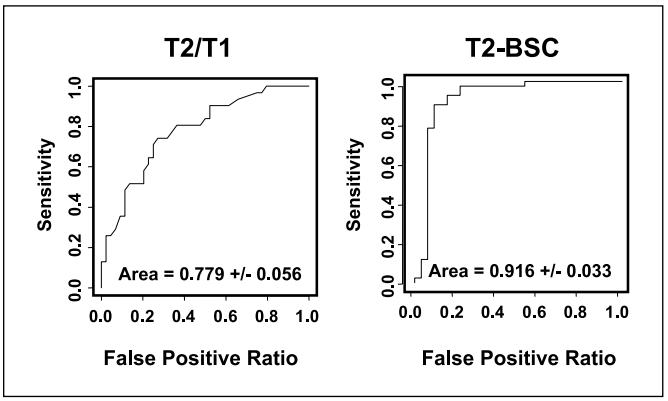

Fig. 4. Receiver operating characteristic curves for T2/T1 and T2 BSC. Receiver operating characteristic curves plotting sensitivity as a function of the false positive ratio (1—specificity) are shown for T2/T1 (*left*) and T2 BSC (*right*). The areas under the curves, which can range from 0.5 if a test has no discrimination and is no better than random chance to 1.0 for a test with perfect discrimination (100% sensitivity and 100% specificity), were 0.78 (T2/T1) and 0.92 (T2 BSC).

T1-enhancing tumor has been attributed to edema, microscopic infiltrative tumor, or both (10). *EGFR*-amplified glioblastomas could exhibit increased surrounding edema because EGFR activation enhances synthesis of hypoxia-inducible transcription factor (16), which in turn promotes increased secretion of cytokines, such as vascular endothelial growth factor, which act as mitogens for endothelial cells and act directly on endothelial cells to increase permeability selectively to proteins (13).

T2-bright signal around tumors may also be explained by microscopic tumor infiltration. In T2-bright white matter beyond tumor margins, as defined by T1 contrast-enhanced MRI, nests of tumor can be identified in stereotactic biopsy specimens (10). Glioma invasion into surrounding white matter is a complex multistep process, likely starting with glioma lysing the extracellular matrix that normally limits cellular migration. Matrix metalloproteinases secreted by gliomas may aid invasion by degrading a broad range of extracellular matrix components surrounding gliomas. Matrix metalloproteinases 1 and 13 are collagenases induced by EGFR signaling and implicated in glioma cell invasion (14). Fibroblast activation protein α, also known as seprase, is an integral membrane serine protease implicated in invasion of which expression is also up-regulated by EGFR signaling (5). In addition, we have shown that there seems to be a microenvironmental selection pressure to retain double minute chromosomal amplicons of the EGFR gene at the invasive edges of glioblastomas (9).

The finding of an increased T2/T1 ratio in tumors overexpressing *EGFR* likely reflects both the increased angiogenesis and edema caused by increased vascular endothelial growth factor secretion and the invasion by these tumors caused by increased expression of matrix metalloproteinases and other proteases. The finding of a decreased T2 BSC in tumors overexpressing *EGFR*, suggesting less sharpness in the T2 border of these tumors, may reflect the increased invasiveness of these lesions.

Another example in which MRI findings correlated with molecular mutations of a tumor was a report documenting that allelic loss of chromosomal arms 1p and 19q in oligodendrogliomas was associated with an indistinct border on T1 images and mixed signal intensity on T1 and T2 images (17). This correlation between tumor molecular analysis and MRI was based on subjective MRI scores rather than on quantitative measures such as the ones we used. The correlation between molecular analysis and MRI described here is the first such correlation for glioblastoma and is based on objective criteria derived from computer-based image analysis that can be done in a reproducible manner by a single person rather than on a subjective review by a panel of experts.

Initial studies correlating MRI findings with histologic features of astrocytic tumors focused on predicting WHO grade, which is of importance because incomplete biopsy sampling of heterogeneous astrocytic tumors could lead to inaccurate grading. Several studies found that MRIs of glioblastomas showed more hemorrhage, cyst formation, necrosis, and contrast enhancement than those of low-grade and anaplastic astrocytomas (18, 19). The present report suggests that, with further volumetric analysis, a preoperative MRI may also enable prediction of molecular glioblastoma subtype.

This is the first reported use of the T2/T1 ratio for MRI analysis. The closest previously published quantitative MRI variable was the vasogenic edema ratio which measured vasogenic edema in hematomas by taking the maximum width of edema outside hematoma on T2 and dividing by the diameter of the hematoma (20). As the vasogenic edema ratio increased, the positive predictive value that there was neoplasm inside the hemorrhage increased. Thus, the zone of T2 brightness on MRI, reflecting edema, is larger around brain tumors than around hematomas. This report expands our understanding of T2 brightness associated with glioblastomas by analyzing three-dimensional volumes rather than two-dimensional diameters and by correlating findings with molecular glioblastoma subtype.

Radiographic necrosis did not vary with glioblastoma subtype and the average necrosis in our glioblastomas was 27%, comparable to a prior report documenting 40% radiographic necrosis on glioblastoma MRIs (21). Glioblastoma radiographic necrosis on MRIs graded on a four-point scale has been reported to inversely correlate with patient survival in a cohort slightly smaller than ours (22) and the presence of any radiographic necrosis represented a negative prognostic factor in a multivariate analysis of over 400 glioblastoma patients in a larger series (23). However, in our patient cohort there was no effect of necrosis on survival, even when patients with no radiographic necrosis were compared with patients with radiographic necrosis. The mechanism of glioblastoma necrosis has not been identified. The lack of correlation between radiographic necrosis and glioblastoma subtype may reflect multiple effects in *EGFR*-amplified glioblastomas that counteract each other. On the one hand, vascular endothelial growth factor–mediated increases in endothelial thromboplastin activity could promote necrosis by inducing intravascular thrombosis leading to infarction (24), and prolonged EGFR activation in cultured cells has been shown to trigger oxidative neuronal injury in adjacent neurons (25). On the other hand, the ability of vessels generated by vascular endothelial growth factor–mediated angiogenesis to perfuse a growing *EGFR*-amplified tumor may reduce the amount of necrosis.

T2/T1 and T2 BSC were not predictive of patient survival. Given the recent finding that *EGFR* genetic changes are not predictive of survival in glioblastoma patients (26, 27), it is not surprising that radiographic variables predictive of *EGFR* amplification also do not correlate with survival. Whereas a radiographic variable predictive of glioblastoma patient survival would be clinically useful, our objective was to identify variables such as T2/T1 and T2 BSC that were predictive of EGFR amplification. These variables are of value for several reasons.

With further analysis, the T2/T1 ratio and T2 BSC may prove to be clinically useful. In a larger data set, a cutpoint T2/T1 or T2 BSC value might be identified through which accurate preoperative predictions of tumor genotype might be possible for some patients. Further studies might also seek radiographic features correlated with expression of the variant III EGFR mutation that is constitutively active with a truncated cytoplasmic domain. EGFR variant III is an independent negative prognostic factor for survival and is overexpressed in 45% of *EGFR*-amplified and in <10% of non-*EGFR*-amplified glioblastomas (28).

Radiographic features such as T2/T1 and T2 BSC that distinguish *EGFR*-amplified from non-*EGFR*-amplified glioblastomas may also eventually contribute to the clinical

management of glioblastoma patients; for example, radiographic features such as those we have identified might predict longer need for corticosteroids in patients with extensive surrounding edema. Radiographic variables might also correlate better with activity of downstream effectors in the EGFR pathway than with levels of EGFR expression. If so, these radiographic variables could potentially lead to better prediction of therapeutic benefit from novel tyrosine kinase inhibitors such as erlotinib (Tarceva) that target EGFR signaling pathways.

Although our results do not allow MRI to replace tissue-based diagnosis, this work begins the process of identifying noninvasive predictors of molecular tumor status for glioblastomas. Our findings of increased T2/T1 ratio and T2 BSC in *EGFR*-amplified glioblastomas also suggest directions for further study of the macroscopic consequences of *EGFR* overexpression in these tumors.

Acknowledgments

We thank Jennifer Roy, Sarah Jhung, David Rhee, and J. Matthew Esposito for technical assistance.

References

1. Randomized trial of procarbazine, lomustine, and vincristine in the adjuvant treatment of high-grade astrocytoma:a Medical Research Council trial. J Clin Oncol 2001;19:509–18.
2. Etienne MC, Formento JL, Lebrun-Frenay C, et al. Epidermal growth factor receptor and labeling index are independent prognostic factors in glial tumor outcome. Clin Cancer Res 1998;4:2383–90.
3. Barker FG, II, Simmons ML, Chang SM, et al. EGFR overexpression and radiation response in glioblastoma multiforme. Int J Radiat Oncol Biol Phys 2001;51:410–8.
4. Schlegel J, Merdes A, Stumm G, et al. Amplification of the epidermal-growth-factor-receptor gene correlates with different growth behaviour in human glioblastoma. Int J Cancer 1994;56:72–7.
5. Lal A, Glazer CA, Martinson HM, et al. Mutant epidermal growth factor receptor up-regulates molecular effectors of tumor invasion. Cancer Res 2002;62:3335–9.
6. Grunwald V, Hidalgo M. Developing inhibitors of the epidermal growth factor receptor for cancer treatment. J Natl Cancer Inst 2003;95:851–67.
7. Bishop PC, Myers T, Robey R, et al. Differential sensitivity of cancer cells to inhibitors of the epidermal growth factor receptor family. Oncogene 2002;21:119–27.
8. Magne N, Fischel JL, Dubreuil A, et al. Influence of epidermal growth factor receptor (EGFR), p53 and intrinsic MAP kinase pathway status of tumour cells on the antiproliferative effect of ZD1839 ("Iressa"). Br J Cancer 2002;86:1518–23.
9. Okada Y, Hurwitz EE, Esposito JM, Brower MA, Nutt CL, Louis DN. Selection pressures of TP53 mutation and microenvironmental location influence epidermal growth factor receptor gene amplification in human glioblastomas. Cancer Res 2003;63:413–6.
10. Kelly PJ, Daumas-Duport C, Kispert DB, Kall BA, Scheithauer BW, Illig JJ. Imaging-based stereotaxic serial biopsies in untreated intracranial glial neoplasms. J Neurosurg 1987;66:865–74.
11. Batchelor TT, Betensky RA, Esposito JM, et al. Age-dependent prognostic effects of genetic alterations in glioblastoma. Clin Cancer Res 2004;10:228–33.
12. Louis DN, Rubio MP, Correa KM, Gusella JF, von Deimling A. Molecular genetics of pediatric brain stem gliomas. Application of PCR techniques to small and archival brain tumor specimens. J Neuropathol Exp Neurol 1993;52:507–15.
13. Maity A, Pore N, Lee J, Solomon D, O'Rourke DM. Epidermal growth factor receptor transcriptionally up-regulates vascular endothelial growth factor expression in human glioblastoma cells via a pathway involving phosphatidylinositol 3′-kinase and distinct from that induced by hypoxia. Cancer Res 2000;60:5879–86.
14. Choe G, Park JK, Jouben-Steele L, et al. Active matrix metalloproteinase 9 expression is associated with primary glioblastoma subtype. Clin Cancer Res 2002;8:2894–901.
15. Simmons ML, Lamborn KR, Takahashi M, et al. Analysis of complex relationships between age, p53, epidermal growth factor receptor, and survival in glioblastoma patients. Cancer Res 2001;61:1122–8.
16. Khatua S, Peterson KM, Brown KM, et al. Overexpression of the EGFR/FKBP12/HIF-2α pathway identified in childhood astrocytomas by angiogenesis gene profiling. Cancer Res 2003;63:1865–70.
17. Megyesi JF, Kachur E, Lee DH, et al. Imaging correlates of molecular signatures in oligodendrogliomas. Clin Cancer Res 2004;10:4303–6.
18. Asari S, Makabe T, Katayama S, Itoh T, Tsuchida S, Ohmoto T. Assessment of the pathological grade of astrocytic gliomas using an MRI score. Neuroradiology 1994;36:308–10.
19. Pierallini A, Bonamini M, Bozzao A, et al. Supratentorial diffuse astrocytic tumours: proposal of an MRI classification. Eur Radiol 1997;7:395–9.
20. Tung GA, Julius BD, Rogg JM. MRI of intracerebral hematoma: value of vasogenic edema ratio for predicting the cause. Neuroradiology 2003;45:357–62.
21. Pierallini A, Bonamini M, Osti MF, et al. Supratentorial glioblastoma:neuroradiological findings and survival after surgery and radiotherapy. Neuroradiology 1996;38 Suppl 1:26–30.
22. Hammoud MA, Sawaya R, Shi W, Thall PF, Leeds NE. Prognostic significance of preoperative MRI scans in glioblastoma multiforme. J Neurooncol 1996;27:65–73.
23. Lacroix M, Abi-Said D, Fourney DR, et al. A multivariate analysis of 416 patients with glioblastoma multiforme:prognosis, extent of resection, and survival. J Neurosurg 2001;95:190–8.
24. Takano S, Tsuboi K, Tomono Y, Mitsui Y, Nose T. Tissue factor, osteopontin, αvβ3 integrin expression in microvasculature of gliomas associated with vascular endothelial growth factor expression. Br J Cancer 2000;82:1967–73.
25. Cha YK, Kim YH, Ahn YH, Koh JY. Epidermal growth factor induces oxidative neuronal injury in cortical culture. J Neurochem 2000;75:298–303.
26. Rich JN, Hans C, Jones B, et al. Gene expression profiling and genetic markers in glioblastoma survival. Cancer Res 2005;65:4051–8.
27. Quan AL, Barnett GH, Lee SY, et al. Epidermal growth factor receptor amplification does not have prognostic significance in patients with glioblastoma multiforme. Int J Radiat Oncol Biol Phys 2005;63:695–703.
28. Shinojima N, Tada K, Shiraishi S, et al. Prognostic value of epidermal growth factor receptor in patients with glioblastoma multiforme. Cancer Res 2003;63:6962–70.

Clinical Cancer Research

Magnetic Resonance Imaging Characteristics Predict Epidermal Growth Factor Receptor Amplification Status in Glioblastoma

Manish Aghi, Paola Gaviani, John W. Henson, et al.

Clin Cancer Res 2005;11:8600-8605.